Optimal control of coupled Josephson qubits

A. Spörl, T. Schulte-Herbrüggen,* and S. J. Glaser

Department of Chemistry, Technische Universität München, Lichtenbergstrasse 4, 85747 Garching, Germany

V. Bergholm

Materials Physics Laboratory, POB 2200 (Technical Physics) FIN-02015 HUT, Helsinki University of Technology, Espoo, Finland

M. J. Storcz, J. Ferber, and F. K. Wilhelm[†]

Physics Department, ASC, and CeNS, Ludwig-Maximilians-Universität, Theresienstr. 37, 80333 Munich, Germany

(Received 28 September 2006; published 2 January 2007)

In two and three coupled Josephson charge qubits, we exemplify how to take pulses for realizing quantum gates from fidelity-limited pioneering stages to the decoherence limit of near time optimal high-fidelity controls. Thus, a CNOT gate can be obtained with a fidelity $>1-10^{-9}$ for the two qubits. Even when including higher charge states, the leakage is below 1%, although the pulses are nonadiabatic. The controls are five times faster than the pioneering experiment [Nature (London) **425**, 941 (2003)] for otherwise identical parameters—i.e., a progress towards the error-correction threshold by a factor of 100. We outline schemes to generate these shaped pulses by Cauer synthesis, or more generally by few LCR circuits. The approach generalizes to larger systems: e.g., directly realizing a TOFFOLI gate in three linearly coupled charge qubits is shown to be 13 times faster than decomposing it into a circuit of nine CNOT gates of the above experimental work. In view of the next generation of fast pulse shapers, the combination of methods is designed to find wide application in quantum control of pseudospin and macroscopic quantum systems.

PACS number(s): 03.67.Lx, 85.25.Cp, 82.56.Jn, 85.35.Gv

I. INTRODUCTION

Aiming at Hamiltonian simulation and quantum computation recent years have seen an increasing array of quantum systems that can be coherently controlled. Next to natural microscopic quantum systems, a particularly attractive candidate for *scalable* setups are superconducting devices based on Josephson junctions [1–3]. Due to the ubiquitous bath degrees of freedom in the solid-state environment, the quantum coherence time remains limited, even in light of recent progress [4,5] approaching theoretical bounds. Thus it is a challenge to generate the gates fast and accurately enough to meet the error correction threshold. This poses fundamental questions, such as (i) to which extent are gate accuracies and speeds limited by the presence of nearby higher levels? (ii) does a constant and relatively strong interaction promote or hinder the gate performance and which parameter is limiting the gate time? and (iii) given the challenge in building control electronics, which properties do pulses for quantum gates in these pseudospin systems have to have?

Recently, progress has been made in applying optimal control techniques to steer quantum systems [6] in a robust, relaxation-minimizing [7] or time optimal way [8,9]. Spin systems are a particularly powerful paradigm of quantum systems [10]: N spins-1/2 are fully controllable, if (i) all spins can be addressed selectively by rf pulses and (ii) if the spins form an arbitrary connected graph of weak (Ising-type)

*Electronic address: tosh@ch.tum.de

†Present address: Institute for Quantum Computing, University of Waterloo, 200 University Ave, Waterloo N2L3G1, Canada; Electronic address: fwilhelm@iqc.ca

coupling interactions. The optimal control techniques of spin systems can be extended to pseudospin systems, such as charge or flux states in superconducting setups, provided their Hamiltonian dynamics can be expressed to sufficient accuracy within a closed Lie algebra, e.g., su(2^N) in a system of N qubits.

II. CONTROLLING THE HAMILTONIAN DYNAMICS OF COUPLED CHARGE QUBITS

As a practically relevant and illustrative example, we consider two capacitively coupled charge qubits controlled by dc pulses as in Ref. [1]. The infinite-dimensional Hilbert space of charge states in the device can be mapped to its low-energy part defined by zero or one excess charge on the respective islands [2]. Identifying these charges as pseudospins, the Hamiltonian can be written as $H_{\text{tot}} = H_{\text{drift}} + H_{\text{control}}$, where the drift or static part reads (for constants see caption to Fig. 1)

$$
\begin{aligned}
H_{\text{drift}} = &-\left(\frac{E_m}{4} + \frac{E_{c1}}{2}\right)(\sigma_z^{(1)} \otimes \mathbb{1}) - \frac{E_{J1}}{2}(\sigma_x^{(1)} \otimes \mathbb{1}) \\
&-\left(\frac{E_m}{4} + \frac{E_{c2}}{2}\right)(\mathbb{1} \otimes \sigma_z^{(2)}) - \frac{E_{J2}}{2}(\mathbb{1} \otimes \sigma_x^{(2)}) \\
&+\frac{E_m}{4}(\sigma_z^{(1)} \otimes \sigma_z^{(2)}),
\end{aligned}
\tag{1}
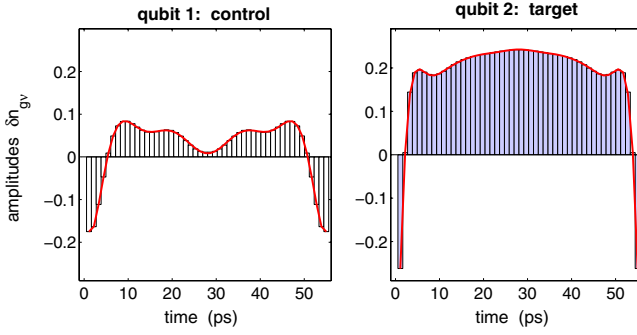$$

while the controls can be cast into

FIG. 1. (Color online) Fastest gate charge controls obtained for realizing a CNOT gate on two coupled charge qubits (left part: control qubit; right part: working qubit). The total gate charges are $n_{g\nu}=n_{g\nu}^0+\delta n_{g\nu}$ with $\nu=1,2$. Here, $n_{g1}^0=0.24$, $n_{g2}^0=0.26$ and the energies $E_{c1}/h=140.2$ GHz, $E_{c2}/h=162.2$ GHz, $E_{J1}/h=10.9$ GHz, $E_{J2}/h=9.9$ GHz, and $E_m/h=23.0$ GHz were taken from the experimental values in [1]. The 50 piecewise constant controls are shown as bars (uniform width $\Delta=t_k=1.1$ ps); the trace fidelity is $(1/2^N)|\mathrm{tr}\{U_{\mathrm{target}}^\dagger U_T\}|>1-10^{-9}$. Red lines give the analytic curves in Eq. (3).

$$H_{\mathrm{control}}=\left(\frac{E_m}{2}n_{g2}+E_{c1}n_{g1}\right)(\sigma_z^{(1)}\otimes\mathbb{1})$$

$$+\left(\frac{E_m}{2}n_{g1}+E_{c2}n_{g2}\right)(\mathbb{1}\otimes\sigma_z^{(2)}). \qquad (2)$$

Note that the Pauli matrices involved constitute a minimal generating set of the Lie algebra su(4); hence the system is fully controllable. The control amplitudes $n_{g\nu}$, $\nu=1,2$ are gate charges controlled by external voltages via $n_{g\nu}=V_{g\nu}C_{g\nu}/2e$. They are taken to be piecewise constant in each time interval t_k. This pseudospin Hamiltonian motivated by Ref. [1] also applies to other systems such as double quantum dots [11] and Josephson flux qubits [12], although in the latter case the controls are typically rf pulses.

In a time interval t_k the system thus evolves under $H_{\mathrm{tot}}^{(k)}:=H_{\mathrm{drift}}+H_{\mathrm{control}}^{(k)}$. The task is to find a sequence of control amplitudes for the intervals $t_1,t_2,\ldots,t_k,\ldots,t_M$ such as to maximize the overlap with the desired quantum gate or element of an algorithm U_{target}. Moreover, for ensuring the decomposition of $U_T=e^{-it_M H_{\mathrm{tot}}^{(M)}}e^{-it_{M-1}H_{\mathrm{tot}}^{(M-1)}}\cdots e^{-it_k H_{\mathrm{tot}}^{(k)}}\cdots e^{-it_1 H_{\mathrm{tot}}^{(1)}}$ into evolutions under the available $\{H_{\mathrm{tot}}^{(k)}\}$ to be time optimal, $T:=\Sigma_{k=1}^M t_k$ has to be minimal. This can be achieved by optimal-control based gradient flows as described in Refs. [13,14].

Throughout the work, we take the parameters from the experiment [1]. Figure 1 shows the fastest decompositions obtained by numerical optimal control for the CNOT gate into evolutions under available controls [Eqs. (1) and (2)]. In contrast to the 255 ps in Ref. [1], $T=55$ ps suffice to get $\|U_T-U_{\mathrm{target}}\|_2=5.3464\times10^{-5}$ corresponding to a trace fidelity of $(1/2^N)|\mathrm{tr}\{U_{\mathrm{target}}^\dagger U_T\}|>1-10^{-9}$ [41].

Figure 2 illustrates how the sequence of controls acts on specific input states [a product state in (a) and a maximally entangled state in (b)] by tracing the quantum evolution on local Bloch spheres (with $\ell\in\{x,y,z\}$ representing $\langle\sigma_\ell\rangle$).

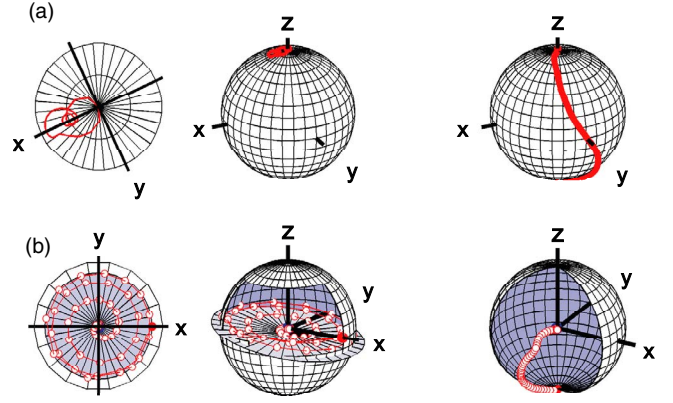

FIG. 2. (Color online) (a) Evolution of the product state $|\Theta(0)\rangle=|0\rangle|0\rangle$ under the optimized controls resulting in $|\Theta(T)\rangle=|0\rangle|1\rangle$. The evolution $0\leq t\leq T$ with $T=55$ ps is represented by the reduced states $\mathrm{tr}_B|\Theta(t)\rangle\langle\Theta(t)|$ (left sphere) and $\mathrm{tr}_A|\Theta(t)\rangle\langle\Theta(t)|$ (right sphere) on the respective local Bloch spheres with the grid lines spaced by $10°$. The blowup shows the top of the left Bloch sphere. (b) Evolution of the Bell state $|\Phi_+\rangle=(1/\sqrt{2})(|00\rangle+|11\rangle)$ into the final state $(1/\sqrt{2})(|01\rangle+|11\rangle)$ (filled red dots). The Bell state is maximally entangled hence in the center of the respective Bloch spheres, while the final state is a product state (filled red dots on the surfaces). The projection on the left is a view from the top.

These pictures trigger physical insight: For a CNOT, the duration $T=55$ ps has to accommodate at least a $\pi/2$ rotation under the coupling Hamiltonian $[(1/2)\sigma_z\otimes\sigma_z]$ lasting 21.7 ps concomitant to two $\pi/2$ x rotations under the drift component $[(1/2)\sigma_x^{(2)}]$ each requiring 25.3 ps. This is in contrast to NMR, where the coupling interactions are some 100 times slower than the local ones. However, in our charge qubit system, the time scales of local and nonlocal interactions are comparable, and the local drifts are even time limiting, while phase shifts are fast [cf. Eqs. (1) and (2)]. Assuming in a limiting simplification that *two* $\pi/2$ x pulses are required, the total length cannot be shorter than 50.6 ps. A sigmoidal phase distortion from a geodesic state inversion is cheap timewise. While the duration of $T=55$ ps of our controls is close to the lower bound of 50.6 ps, the controls in Ref. [1] last 255 ps; they entail several closed great circles on the Bloch sphere and are far from geodesic as obvious from Fig. 3.

Note that the time course of controls turns out palindromic (Fig. 1). Self-inverse gates ($U_{\mathrm{gate}}^2=\mathbb{1}$) relate to the more general time-and-phase-reversal symmetry observed in the control of spin systems [15]: For example, any sequence $e^{-it_x\sigma_x}e^{-it_y\sigma_y}e^{-it_z\sigma_z}$ is inverted by transposition concomitant to time reversal $t_\nu\mapsto-t_\nu$ and $\sigma_y\mapsto-\sigma_y$. Since the Hamiltonians in Eqs. (1) and (2) are real and symmetric, they will give the same propagator, no matter whether read forward or backward.

Let F denote the fidelity of a gate of duration T, and let T_2 be the pertinent overall decay time. Assuming independent errors, the quality is $q\simeq Fe^{-T/T_2}$, where the error rate $1-q\simeq10^{-4}$ is an estimate for the error-correction threshold. With the pulses presented here, the total error rate amounts to $1-q=0.0055$, instead of $1-q=0.5917$ in the pioneering setting [1].
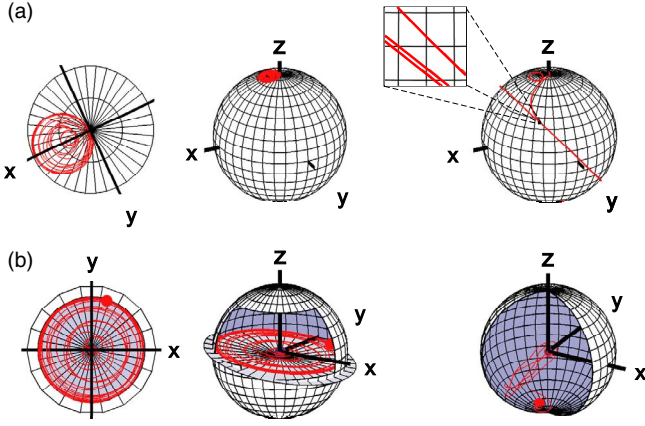
FIG. 3. (Color online) Same as Fig. 2, but with pulses of the experiment taking 255 ps [1]. The trajectory in (b) completes two full circles (see inset) before reaching its final state near the south pole. Grid lines are spaced by 10° on the Bloch spheres and by 1° in the inset.

A visualization complementary to the local Bloch spheres is provided by the Weyl chamber [16] of Fig. 4: It solely picks out the coupling evolution in the factor space [8,17] $G/K=\mathrm{SU}(4)/\mathrm{SU}(2)^{\otimes 2}$. Whereas in NMR time scales, the coupling evolution is time limiting and time optima are thus geodesics [8] in G/K, here in the charge qubits, local and nonlocal evolutions take similar times thus giving a mildly recurrent curve in the Weyl chamber under the optimized controls (a), while under the rectangular pulses used in the pioneering work [1] it goes back and forth (b).

With the pulse shapes on either qubit ($\nu=1,2$) being palindromic, they can be written as a cosine Fourier series
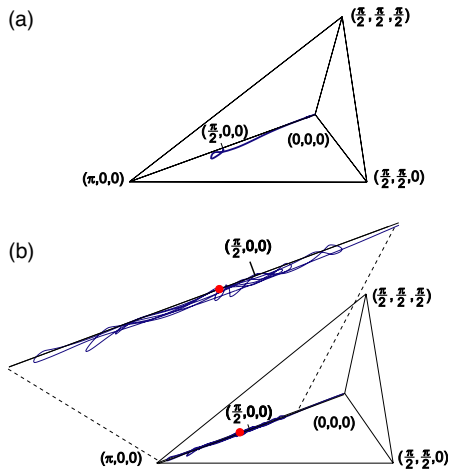

FIG. 4. (Color online) Coupling evolution under the controls of Fig. 1 represented in the Weyl chamber. With local and nonlocal controls being of comparable time scale, where the time for a *local* π pulse is actually time limiting, the time-optimized controls (a) give a mildly recurrent smooth curve which ends at the point $(\pi/2,0,0)$ as expected for a CNOT requiring a $\pi/2$ evolution under the coupling term $(1/2)\sigma_z\otimes\sigma_z$. In contrast, the coupling evolution under the controls of Ref. [1] is meandering back and forth (b) and terminates (red dot) without reaching $\pi/2$ exactly.

$$n_{g\nu}(t) = \sum_{\ell=0}^{19} a_\nu(\ell)\cos\left(2\pi\ell\,\frac{t-T/2}{T}\right), \qquad (3)$$

where 20 components (listed in Table I) suffice to give high accuracy. Alternatively, the pulse shapes can be generated by superimposing short Gaussian, single-flux quantum (SFQ) pulses [18] or rapid SFQ pulses [19], where the coupling strength determines the minimal pulse length.

III. PULSE SHAPING HARDWARE

In the pertinent time scale, commercial devices for generating arbitrary wave forms are not available. Yet high-end pulse generators [20,21] or ultrafast classical Josephson electronics [19,22] are close to the necessary specifications.

A. Overview

As a proof of principle, it is important to note on a general scale how to generate these pulses experimentally, which can readily be exemplified using the well-established technique of pulse shaping in Laplace space [23]: One starts with an input current pulse $I_{\mathrm{in}}(t)$ shorter than the desired one. Its shape may be arbitrary as long as it contains enough spectral weight at the harmonics necessary for the desired pulse. Such pulses can be generated optically or electrically [21]. They serve as input to a discrete electrical two-terminal element with transfer function Z_{12} to be designed for the desired output shape. In Laplace space, the output signal takes the form $V_g(s) := Z_{12}(s)I_{\mathrm{in}}(s)$. So the gate voltages $V_g(t)$ (as in Fig. 1) are Laplace transformed to $\hat{V}_g(s)$ in order to determine the transfer function $Z_{12}(s)$ by fitting $V_g(s)$ to $\hat{V}_g(s)$ given the input pulse $I_{\mathrm{in}}(s)$. However, here in the special case of palindromic pulse shapes expressed by a cosine Fourier series [see Eq. (3)], Z_{12} is already directly given by a series of Lorentzians, viz. the Laplace transform of the cosine series. This results in the particularly simple circuit networks of 20 reactive LC filters shown in Fig. 5. They match the desired pulse shapes extremely well (see Fig. 1) giving a trace fidelity of $1-10^{-5}$ for the entire CNOT. However, compensating for a frequency-dependent transfer function from the generator to the sample, which has to be precisely determined for the respective experimental setting, requires the above more general approach.

B. General approach

Apart from giving details, this section generalizes the pulse shaping schemes outlined above. The network of filters can be obtained by Laplace transforming the gate voltages $V_g(t)$ obtained from optimal control theory to $\hat{V}_g(s)$. Then the transfer function $Z_{12}(s)$ is determined by fitting a $V_g(s)$ to $\hat{V}_g(s)$ in Laplace space, where $V_g(s)=Z_{12}(s)I_{\mathrm{in}}(s)$.

Now criteria of realizibility of standard network synthesis [23,24] apply. A standard two-terminal element is created by input and output impedances Z_{11} and Z_{22} as well as transfer functions Z_{12} and Z_{21}. A pulse shape can be realized by a passive LCR two-terminal element (where, henceforth,

TABLE I. Translation of the Fourier coefficients $a_{1,2}(\ell)$ of the cosine series expansion [Eq. (3)] of the pulse shape for both qubits found by optimal control $[n_{g\nu}(t)]$ into the parameters of the circuit network for shaping the pulse (Fig. 5). The duration of the shaped output pulse is $T = 55$ ps, while a rectangular current pulse of the same length of 55 ps is used as input. Similar results hold for any on-off pulse as the ones generated by ultrafast flip-flops such as the TFF [22]. For normalization of the impedances $\omega_0 = 2\pi/T = 2\pi \times 18.2$ GHz and $R_{0,1} = 1.17k\ \Omega$, $R_{0,2} = 603\ \Omega$ have been chosen so that for the main frequency at $\ell = 1$ the circuit is matched to $50\ \Omega$ impedance, thus being in accordance with typical superconducting charge qubit frequencies and electrical high level sources. Due to this matching condition the values of C_1 and L_1 ($\ell = 1$) are identical for qubit 1 and qubit 2. The pulses from network synthesis match the desired pulse shape with $\chi^2 = 0.000\,081\,320$ (first qubit) and $\chi^2 = 0.002\,089\,946$ (second qubit), respectively. The simulated fidelity obtained from the pulse sequence expressed via this Fourier decomposition is $F = 0.99\,997\,805$.

	Qubit 1				Qubit 2			
ℓ	$a_1(\ell)\ (10^{-2})$	C_ℓ (fF)	L_ℓ (pH)	$t_{1\ell}$	$a_2(\ell)\ (10^{-2})$	C_ℓ (fF)	L_ℓ (pH)	$t_{2\ell}$
0	2.3445	318.3603		1	18.5266	78.3569		1
1	4.2633	175.0704	437.6761	−1	8.2920	175.0704	437.6761	−1
2	−6.9807	53.4606	358.3209	−1	−4.9516	146.5863	130.6809	−1
3	3.9959	62.2623	136.7408	−1	4.4588	108.5254	78.4498	−1
4	−3.8557	48.3952	98.9563	−1	−4.4322	81.8828	58.4861	−1
5	1.4294	104.4348	29.3481	−1	4.4960	64.5769	47.4623	−1
6	−0.3707	335.5804	6.3426	−1	−4.0870	59.1986	35.9544	−1
7	0.1844	578.2083	2.7045	−1	3.4886	59.4460	26.3055	−1
8	0.0675	1382.8464	0.8658	1	−2.9192	62.1604	19.2607	−1
9	−0.1152	719.5833	1.3146	1	2.4259	66.4889	14.2276	−1
10	0.1707	437.1645	1.7528	1	−2.0116	72.1667	10.6177	−1
11	−0.1510	449.3288	1.4093	1	1.6640	79.3116	7.9844	−1
12	0.1499	414.8163	1.2828	1	−1.3829	87.4772	6.0829	−1
13	−0.1175	488.8320	0.9275	1	1.1498	97.1160	4.6686	−1
14	0.1039	513.0812	0.7619	1	−0.9614	107.8496	3.6249	−1
15	−0.0752	662.0660	0.5144	1	0.8033	120.4750	2.8267	−1
16	0.0663	703.9375	0.4252	1	−0.6702	135.3691	2.2111	−1
17	−0.0448	979.9308	0.2706	1	0.5537	154.2253	1.7191	−1
18	0.0438	947.3556	0.2496	1	−0.4576	176.2347	1.3419	−1
19	−0.0251	1567.1105	0.1354	1	0.3965	192.6855	1.1016	−1

L,C,R, denote inductivity, capacity and resistance, respectively), if in Laplace space (with $s := \sigma + i\omega$) the pertinent transfer function $Z_{12}(s)$ can be found such that the determinant $H(s) = Z_{11}Z_{22} - Z_{12}Z_{21}$ as well as the input and output impedances alone can be written as fractions of polynomials $H(s) = P(s)/Q(s)$ such that in each case (1) $H(s)$ is a real-valued rational function, (2) $Q(s)$ is a Hurwitz polynomial [42], (3) the degree of $P(s)$ does not exceed the degree of $Q(s)$, and (4) $|H(i\omega)| \leq 1$.

Conditions (2) and (3) exclude that the $H(s)$ have poles in the right half-plane. Note that many important time-domain functions, such as, e.g., the trigonometric functions, the Heaviside function, the Dirac delta function, and the exponential function are expressed as rational functions in Laplace space. Thus a wide range of pulse shapes in time domain is accessible by circuit synthesis. Importantly, the transmission functions of typical coaxial cables used to interconnect the different parts of the experimental setup give rise to damping and thus introduce dissipative (i.e., resistive) elements in the circuit, the main physical limitation being that the bandwidth of the output cannot be greatly enhanced relative to the input. The maximum enhancement originates from a series inductor with $Z = sL$. Thus the spectral content

required at the output must be contained in the input as this scheme is essentially subtractive synthesis.

With the corresponding decomposition, there are a number of ways for designing a lumped circuit for a given transfer function, e.g., the method of Gewertz [25] that systematically eliminates poles and introduces loops in the electrical circuit. Iteratively the circuit is synthesized from basic building blocks: One LCR loop for each pair of complex conjugate poles, and one RC filter for each pole on the real axis. Note that in Laplace space the degree of both the nominator and the denominator polynomial of the transfer function Z_{12} approaches the same limiting value for large values of s.

1. Cauer synthesis for controls with time reversal symmetry

In the special case of a real symmetric Hamiltonian allowing for a palindromic pulse sequence, the transfer function $Z_{12}(s)$ is directly obtained by the Laplace transform of the cosine series representation of the control pulses thus circumventing the above numerical fitting procedure in Laplace space. In order to simplify the circuit, we chose $Z_{11} = Z_{22} = Z_{12} = Z_{21}$. This condition can be dropped at the expense of additional inductors if more elaborate impedance matching is
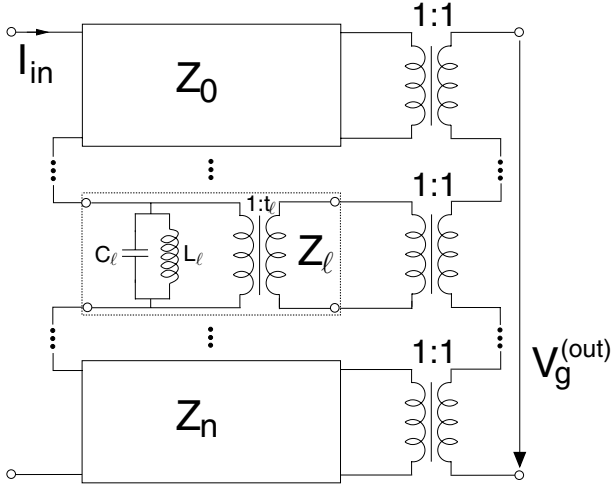
FIG. 5. Circuit network for pulse shaping by Cauer synthesis via the Laplace transform of the cosine Fourier series of Eq. (3), so $Z_{12} = \Sigma_\ell a_\nu(\ell)(-1)^\ell s / [s^2 + (2\pi\ell/T)^2]$. I_{in} is the input current pulse (here 55 ps) and $V_g(s) = Z_{12}(s)I_{in}(s)$ relates to gate voltages $n_{g\nu} = C_{G,\nu}V_{out,\nu}/2e$ on qubits $\nu = 1,2$. All the values $a_\nu(\ell)$, L_ℓ, and C_ℓ are tabulated in Table I.

desired. We take the Heaviside-type rectangular input pulse $I = I_0[\Theta(T) - \Theta(0)]$. The method applies to all toggle-style pulses of the form $I = \tilde{I}(t) - \tilde{I}(T-t)$, where $\tilde{I}$ is an arbitrary function of sufficient bandwidth. For the pulses presented in Fig. 1, Table I gives the Fourier amplitudes of the cosine-series decompositions according to Eq. (3) translated into the parameters for the reactive circuit elements of Fig. 5. The values are obtained from a Fourier series decomposition of the pulse shapes from optimal control $n_{g_\nu}(t) = \Sigma_{\ell=0}^{19} a_\nu(\ell)\cos[2\pi\ell(t-T/2)/T]$ with an appropriate basic frequency $\omega_0 = 2\pi/T$. For the Cauer synthesis, the terms in the polynomial $Z_{12}(s)$ can be split into terms that either give a capacitive circuit element, an inductive circuit element or a parallel circuit of both capacitances and inductances. These circuit elements are normalized with respect to both frequency and resistance according to $C_{\ell,norm} = C_\ell(R_0\omega_0)$ and $L_{\ell,norm} = L_\ell(\omega_0/R_0)$ [23]. Here $R_{0,1} = 1.17$ kΩ, $R_{0,2} = 603$ Ω, and $\omega_0 = 2\pi/T = 2\pi \times 18.2$ GHz have been used for normalization. This leads to a typical impedance for the fundamental frequencies of order 50Ω thus matching typical coaxial cables. (More detailed modeling requires taking the output level of the pulse generator into account.)

The numerical values for the reactive circuit elements are obtained by Cauer synthesis, namely $C_\ell = [\ell|a_\nu(\ell)|]^{-1}$, $L_\ell = T_0|a_\nu(\ell)|^2/(2\pi\ell)$, and $t_\ell = \text{sgn}[(-1)^\ell a_\nu(\ell)]$. Both parts of the table show a Cauer network synthesis with experimentally feasible values for the reactive elements, which at these frequencies can, e.g., be realized by the on-chip cavitylike structure of variable width and length adjusting capacitances and inductances from the simulated time evolution of the CNOT gate. Under the synthesized controls a fidelity of $F = 1 - 10^{-5}$ is obtained without taking leakage and decoherence into account.

We want to emphasize that since palindromic pulse controls can be written as a cosine series, the Cauer synthesis

translates them into a network solely made of capacitive and inductive elements, which are nondissipative thus reducing the heat load on the circuit.

C. Additional compensation for nonideal transfer functions

Moreover, in view of concrete experiments, the transfer function from the pulse shaping unit to the qubit can be measured, e.g., by using a capacitor that mimics the qubit. In the linear case, it takes the form of another four-pole impedance matrix Z_{sample}. The total transfer function of the series configuration of those four poles then reads $Z_{12}^{(full)} := Z_{12,sample}Z_{12,filter}/(Z_{22,filter} + Z_{11,sample})$. For the experimental setup it suffices to make sure the transfer function to the sample is not filtering out the relevant frequencies (i.e., becomes small for values of s important to $V_g^{(out)}$): Then one may readily design a filter compensating for specified experimental imperfections so that finally the *full* transfer function $Z_{12}^{(full)}$ is taken into account for shaping the pulse. In general, however, $Z_{12}^{(full)}$ will also contain dissipative elements, which means it cannot be obtained by the particularly simple Cauer synthesis. Note that in general network synthesis the poles of $Z_{12}^{(full)}(s)$ have to be investigated carefully and the circuit network will be more complex than the one shown in Fig. 5, yet it can still be split into basic circuits corresponding to the different poles of $Z_{12}(s)$.

Due to unavoidable fabrication uncertainties, the optimum pulse will be slightly different for each individual pair of qubits. Thus the parameters for the Hamiltonians in Eqs. (1) and (2) have to be determined spectroscopically before re-running our algorithm to adapt the optimal pulse shapes.

Importantly, pulses can also be formed by means of superimposing short pulses of shapes that are generated with different heights, widths, and delays. The two main candidates for this approach are (i) Gaussian pulses [11], which can be generated at room temperature and pass the necessary cryogenic filtering nearly undistorted, and (ii) SFQ pulses (*vide supra*), which can be generated on chip (hence avoiding the filters) using ultrafast classical Josephson electronics [22]. The pulse sequences obtained in this work can be fitted very well by superpositions of a few Gaussian or harmonic pulses still leading to fidelities >0.999.

Note that our optimization method also applies to control by microwave Rabi-type pulses [3], where pulse shaping appears to be easier as time scales are usually longer.

IV. LOW LEAKAGE AND ROBUSTNESS OF OPTIMIZED CONTROLS

The limited bandwidth allows us to maintain high fidelity even if leakage levels formed from higher charge states of the qubit system are taken into account: We now explicitly apply the pulses to the extended system obtained by mapping the full Hamiltonian [1] to the subspaces of $-1, \ldots, 2$ extra charges per island. The two-qubit CNOT gate is thus embedded into the group SU(16); still the full propagator generated by the above controls projects onto the CNOT gate giving a trace fidelity >0.99. Even the time courses starting with any of the four canonical two-qubit basis vectors hardly ever
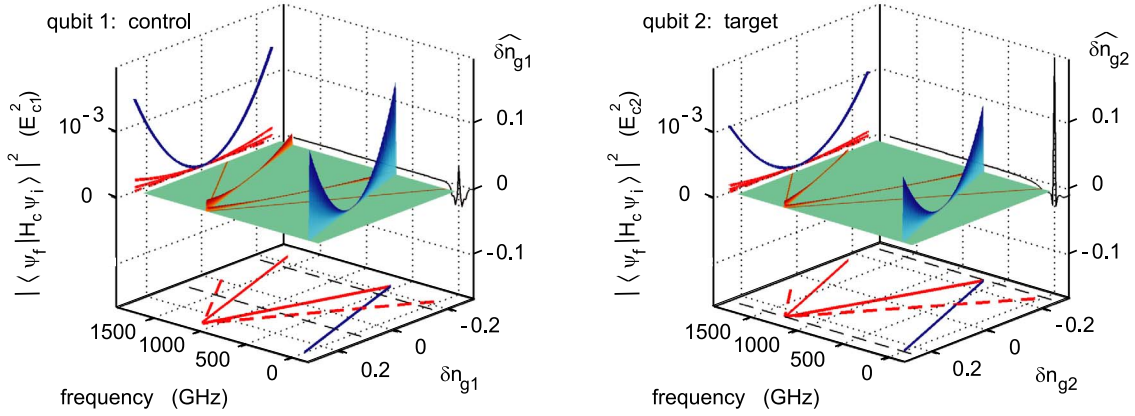
FIG. 6. (Color online) Spectroscopic explanation of the high quality of the optimized pulse controls: The spectral overlap of the Fourier transforms (right walls) of the controls of Fig. 1 with the energy differences corresponding to the one-charge transitions into leakage levels (solid lines on the surface) is small at gate charges in the working range (within black dashed lines) around $\delta n_{g\nu} \simeq 0.2$ ($\nu = 1, 2$) corresponding to $n_{g\nu} \simeq 0.45$. In the 3D representation, intensities at allowed (solid lines) vs forbidden transitions (broken lines) into leakage levels are given in terms of transition-matrix elements (normalized by charging energies E_{c1}^2, E_{c2}^2) with an extended control Hamiltonian expressed by $H_c(\delta n_{g\nu})$ in $|\langle \Psi_f | H_c \Psi_i \rangle|^2$: The working transitions (blue) are far more probable than the allowed ones into leakage levels (red) that have no overlap with the excitation bandwidth of the pulses; the forbidden transitions are but spurious.

leave the state space of the working qubits: At no time do the projections onto the leakage space exceed 0.6%. Clearly, optimization including explicit leakage levels could improve the quality even further in systems where necessary [26].

As illustrated in Fig. 6, in simplified terms, the high quality can be understood by relating the limited bandwidth to the transitions between the eigenstates of the local parts of H_{drift} in Eq. (1): While *one-charge* transitions to leakage levels like $|-1\rangle \leftrightarrow |0\rangle$ and $|2\rangle \leftrightarrow |1\rangle$ are allowed, *two-charge* transitions like $|-1\rangle \leftrightarrow |1\rangle$ and $|2\rangle \leftrightarrow |0\rangle$ are forbidden in terms of the transition-matrix elements $|\langle \Psi_{\text{final}} | H_{\text{control}} \Psi_{\text{initial}} \rangle|^2$. Note the charge control on gate 2 in Fig. 1 is around $\delta n_{g2} = 0.2$ thus driving the working transition $|0\rangle \leftrightarrow |1\rangle$, while the "spectral overlap" of the Fourier transform of the time course in both controls with energy differences corresponding to one-charge leakage transitions is small. Hence simple spectroscopic arguments underpin the high fidelity.

Moreover, our controls are notably robust with regard to $\pm 5\%$ variation of the tunneling frequencies $E_{J_{1,2}}$ and the coupling term E_m as well as to Gaussian noise on the control amplitudes and time intervals as shown in Fig. 7. Variations of the tunneling energies $E_{J\nu}$ ($\nu = 1, 2$) may result from imperfections in the junction oxide as well as deviating cou-

pling strength E_m. These parameters have to be determined spectroscopically, where the relative error normally does not exceed 5%. Even the time-optimized controls as short as $T = 55$ ps cope with such variations. Significant improvement of the broadband behavior, however, could not be obtained by pulse sequences up to a total duration of $T = 75$ ps, thus suggesting that broadband CNOT controls tailored for the special (and rare) instances with ill-defined experimental parameters will require considerably longer pulse schemes. Similar robustness is observed against Gaussian noise on the control amplitudes or time units.

V. TOFFOLI GATE FOR THREE LINEARLY COUPLED QUBITS

Likewise, in a system of three linearly coupled charge qubits, we determined a realization of the TOFFOLI gate with experimentally available controls (Fig. 8), where the speed-up against a circuit of nine CNOT gates is by a factor of 2.8 with our CNOT and by 13 with the CNOT gates of Ref. [1].

In a linear chain of three coupled qubits, a TOFFOLI gate needs nine CNOT gates, which gives an error rate of $1 - q_{\text{pioneer}} = 1 - 0.4083^9 = 0.9997$ using the CNOT of Ref. [1],
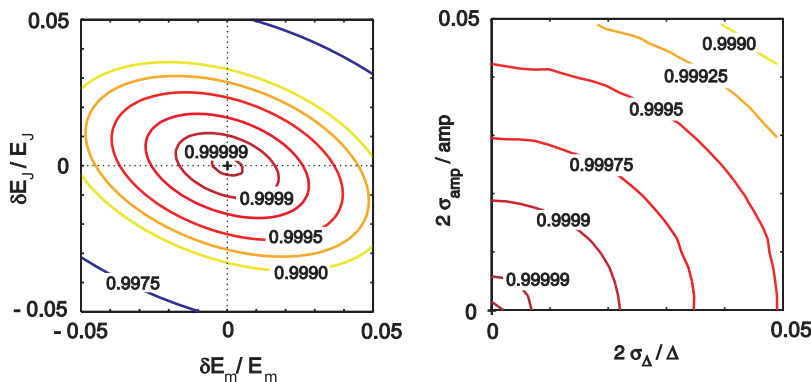

FIG. 7. (Color online) Left: Trace fidelities under controls of Fig. 1 when the parameters E_m and E_J in Eqs. (1) and (2) vary by $\pm 5\%$. Right: Fidelities under Gaussian noise on control amplitudes and time intervals parametrized by the standard deviations $2\sigma_\Delta/\Delta$ and $2\sigma_{\text{amp}}/\text{amp}$ ranging from 0 to 5%. (As in Fig. 1, $\Delta := t_k$; amp $:= \delta n_{g\nu}$ with $\nu = 1, 2$.) Each data point is an average of 25 000 Monte Carlo simulations.
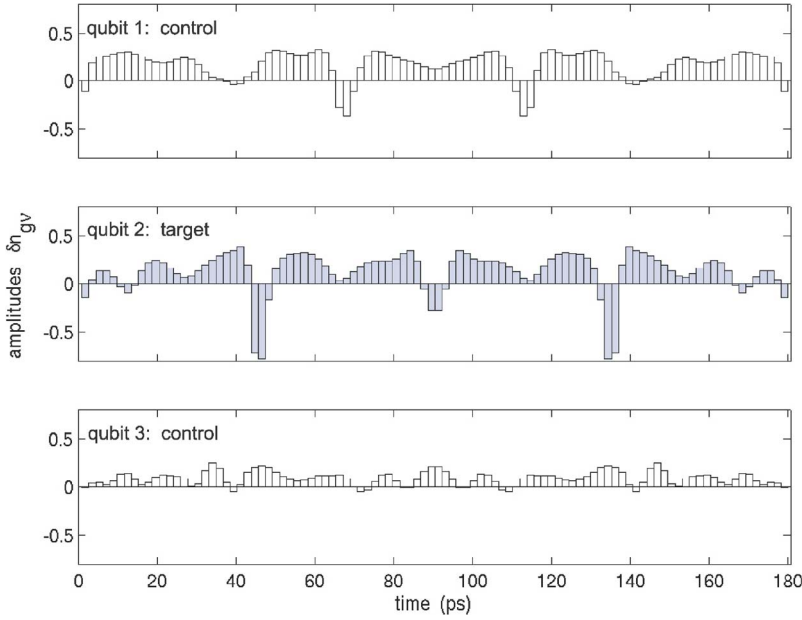
FIG. 8. (Color online) Fastest gate charge controls obtained for realizing a TOFFOLI gate on a linear chain of charge qubits coupled by nearest-neighbor interactions with a trace fidelity of $(1/2^N)|\mathrm{tr}\{U_{\mathrm{target}}^\dagger U_T\}| > 1-10^{-5}$. Parameters: $E_{c1}/h=140.2$ GHz, $E_{c2}/h=120.9$ GHz, $E_{c3}/h=184.3$ GHz, $E_{J1}/h=10.9$ GHz, $E_{J2}/h=9.9$ GHz, $E_{J3}/h=9.4$ GHz, $E_{m1,m2}/h=23$ GHz, $n_{g1}^0=0.24$, $n_{g2}^0=0.26$, and $n_{g3}^0=0.28$.

an error rate of $1-q_{\mathrm{network}}=1-0.9945^9=0.0483$ with nine of our CNOT, while the error rate of the TOFFOLI gate shown in Fig. 8 is $1-q_{\mathrm{direct}}=1-0.99999e^{-180\ \mathrm{ps}/10\ \mathrm{ns}}=0.0178$, assuming for the moment that the T_2 in a coupled three-qubit Josephson system would also be in the order of 10 ns.

Due to the quite strong qubit-qubit interactions in multi-qubit setups, generating three-qubit gates directly is much faster than by universal gates. This also holds in simple algorithms [27] on superconducting qubit setups: A minimization algorithm for searching control amplitudes in coupled Cooper pair boxes was applied in [28], where the optimization was restricted to very few values. In Ref. [29], a rf-pulse sequence for a CNOT with fixed couplings was introduced, to which optimal control could be applied likewise: The sequence is longer using more of the available decoherence time, which is partly (but not fully) compensated by the longer T_2 at the optimum point. For the charge-qubit setting here, the control techniques lead to a time-optimized gate that can be performed some 200 times within a nonoptimum point T_2^* of 10 ns.

VI. TOWARD THE ERROR-CORRECTION THRESHOLD: GUIDELINES AND FRONTIERS AHEAD

It is the main purpose of this section to make a strong case for the next generation of fast pulse shapers. Actually we regard them as paramount for reaching the goal of scalable quantum computation with superconducting Josephson elements. Let F denote the fidelity of a gate of duration T, and let T_2 be the pertinent overall decay time. Assuming independent errors, the quality of a gate is roughly determined by $q \simeq F e^{-T/T_2} \simeq F(1-T/T_2)$, where the error rate $1-q \simeq 10^{-4}$ is an estimate for the error-correction threshold (see, e.g., [30]). This goal can be met by improvements on three frontiers: (1) Fighting decoherence by making T_2 longer, (2) cutting gate times by making T shorter, and (3) improving fidelity by making F larger, where this work shows how to exploit op-

timal control for getting to the limits in the latter two.

(1) In fact the Josephson devices known today [1,3,4] have already undergone a great deal of hardware optimization bringing decoherence down close to its theoretical limits. The observed decoherence times in charge qubits are on the scale of $T_2 \simeq 0.5$ to 2.5 ns for two-qubit dynamics [31], and 10 ns for single qubits [32]. Both can be improved by using echo techniques [33], which hints at $1/f$ noise as the limiting factor. Other improvements of T_2 rely on operating with microwave pulses [3,34] at an optimum bias point at the expense of much slower pulses limited by the Rabi frequency. Although our technique may incorporate both strategies, echo and microwave pulses, we base our technological estimate in the next section on an optimistic T_2 of 10 ns, which appears to be accessible in a charge qubit setup as in [1].

(2) The pulse controls *currently available* are too slow to fully exploit the potential of the experimental setting: Within a decay time of 10 ns, just 40 CNOT gates of the current duration of 255 ps can be performed (with the rise times in the order of 35 ps). On the other hand, the capacitively coupled Josephson hardware elements themselves have large intrinsic frequency scales allowing for fast operation and may well reach the decoherence-limited threshold—provided gates could be executed some 10 times faster than in the current experimental setting, where we have shown that, within 10 ns, approximately 200 time-optimized high-fidelity CNOT can be run.

(3) For obtaining sufficiently high fidelities experimentally, an important part of the future challenge will be the accurate determination of the experimental system response: Once this can be done, a nonideal system response can easily be incorporated into our algorithms thus allowing for getting fidelities that are essentially limited by the robustness of the experimental setting. With fidelities of F up to $1-10^{-9}$ being ideally accessible by our pulses, the total error rate is then entirely limited by decoherence (T/T_2).

A. Guidelines

Our results make a strong case for faster pulse generation, both shorter in total length and with the possibility of shaping the external structure. This is a cornerstone for future progress and needs to be combined with the current strategies such as decoherence engineering and the optimal working point. In particular, even though the current experimental controls [1] could further be optimized for higher fidelity, a simple estimate shows that this will not suffice for significant improvements given the time scales of current pulse shaping technology: In the case of a CNOT, the quality would always be limited by $e^{-T/T_2}=0.975$ even at fidelities of $F=1$. On the same footing, if higher fidelity is achieved by additional compensation pulses [35–38], the total sequence becomes longer and the quality again deteriorates. The optimal working point strategy works excellent for single qubits [34] but becomes difficult for two-qubit operations, which also appear to be slow [29,39]. Rather, by making the Josephson hardware system even faster without introducing higher T_2 decay rates, high quality gates can be achieved by optimized fast control alone, even if the optimal point is not invoked. Realistically, a combination of optimal control, optimal point, and refocusing may be most powerful and accessible. Clearly, this technological frontier has not been really explored so far, yet the time scales needed are not excessively short compared to what has been realized with electro-optical methods involving pulsed lasers and switches [40]. For getting sufficiently high fidelities experimentally, it will be crucial to accurately determine the experimental system response, which should then be included into the numerical algorithms.

VII. CONCLUSION

We have shown how to take pulse controls for realizing quantum gates in pseudospin systems from fidelity-limited pioneering stages to the decoherence limit of near time optimal high-fidelity controls. In superconducting charge qubits, the progress towards the error-correction threshold is by a factor of 100. Limiting the optimal-control based shapes to low bandwidth allows for nonadiabatic pulses with remarkably low leakage to higher states thus justifying the two-level truncation to the low-energy part of the spectrum. Moreover, shapes could be kept simple enough to be realized by Cauer synthesis or a few LCR circuits. So the approach will find wide application, in particular for the next generation of fast pulse-shaping devices.

We expect T_2 time scales dominated by $1/f$ contributions will not change largely under the pulses, so time optimal controls provide a significant step towards the accuracy threshold for quantum computing, even if cutting decoherence times reaches its intrinsic limits.

[1] T. Yamamoto, Y. A. Pashkin, O. Astafiev, Y. Nakamura, and J. S. Tsai, Nature (London) **425**, 941 (2003).

[2] Y. Makhlin, G. Schön, and A. Shnirman, Rev. Mod. Phys. **73**, 357 (2001).

[3] R. McDermott, R. W. Simmonds, M. Steffen, K. B. Cooper, K. Cicak, K. D. Osborn, S. Oh, D. P. Pappas, and J. M. Martinis, Science **307**, 1299 (2005).

[4] P. Bertet, I. Chiorescu, G. Burkard, K. Semba, C. Harmans, D. DiVincenzo, and J. Mooij, e-print cond-mat/0412485.

[5] O. Astafiev, Y. A. Pashkin, Y. Nakamura, T. Yamamoto, and J. S. Tsai, Phys. Rev. Lett. **93**, 267007 (2004).

[6] A. G. Butkovskiy and Y. I. Samoilenko, *Control of Quantum-Mechanical Processes and Systems* (Kluwer, Dordrecht, 1990).

[7] N. Khaneja, B. Luy, and S. J. Glaser, Proc. Natl. Acad. Sci. U.S.A. **100**, 13162 (2003).

[8] N. Khaneja, R. Brockett, and S. J. Glaser, Phys. Rev. A **63**, 032308 (2001).

[9] N. Khaneja, S. J. Glaser, and R. Brockett, Phys. Rev. A **65**, 032301 (2002).

[10] S. J. Glaser, T. Schulte-Herbrüggen, M. Sieveking, O. Schedletzky, N. C. Nielsen, O. W. Sørensen, and C. Griesinger, Science **280**, 421 (1998).

[11] T. Hayashi, T. Fujisawa, H. D. Cheong, Y. H. Yeong, and Y. Hirayama, Phys. Rev. Lett. **91**, 226804 (2003).

[12] J. B. Majer, F. G. Paauw, A. C. J. ter Haar, C. J. P. M. Harmans, and J. E. Mooij, Phys. Rev. Lett. **94**, 090501 (2005).

[13] N. Khaneja, T. Reiss, C. Kehlet, T. Schulte-Herbrüggen, and S. J. Glaser, J. Magn. Reson. **172**, 296 (2005).

[14] T. Schulte-Herbrüggen, A. Spörl, N. Khaneja, and S. J. Glaser, Phys. Rev. A **72**, 042331 (2005).

[15] C. Griesinger, C. Gemperle, O. W. Sørensen, and R. R. Ernst, Mol. Phys. **62**, 295 (1987).

[16] S. Helgason, *Differential Geometry, Lie Groups, and Symmetric Spaces* (Academic Press, New York, 1978).

[17] J. Zhang, J. Vala, S. Sastry, and K. B. Whaley, Phys. Rev. A **67**, 042313 (2003).

[18] P. Bunyk, K. Likharev, and D. Zinoviev, Int. J. High Speed Electron. Syst. **11**, 257 (2001).

[19] A. B. Zorin, E. M. Tolkacheva, M. I. Khabipov, F. I. Buchholz, and J. Niemeyer, Phys. Rev. B **74**, 014508 (2006).

[20] H. Kim, A. Kozyrev, S. Ho, and D. van der Weide, IEEE MTT-S International Microwave Symposium Digest **4**, 1945 (2005).

[21] H. Qin, R. Blick, D. van der Weide, and K. Eberl, Physica E (Amsterdam) **13**, 109 (2002).

[22] D. Brock, Int. J. High Speed Electron. Syst. **11**, 307 (2001).

[23] W. Rupprecht, *Netzwerksynthese* (Springer, Berlin, 1972).

[24] G. C. Temes and J. W. LaPatra, *Introduction to Circuit Synthesis and Design* (McGraw-Hill, New York, 1977).

[25] C. Gewertz, J. Math. Phys. **12**, 1 (1932).

[26] S. Sklarz and D. Tannor, e-print quant-ph/0404081; Chem. Phys. **322**, 87 (2006).

[27] J. Vartiainen, A. Niskanen, M. Nakahara, and M. Salomaa, Int. J. Quantum Inf. **2**, 1 (2004).

[28] A. O. Niskanen, J. J. Vartiainen, and M. M. Salomaa, Phys. Rev. Lett. **90**, 197901 (2003).

[29] C. Rigetti, A. Blais, and M. Devoret, Phys. Rev. Lett. **94**, 240502 (2005).

[30] M. Nielsen and I. Chuang, *Quantum Computation and Quantum Information* (Cambridge University Press, Cambridge, UK, 2000).

[31] Y. A. Pashkin, T. Yamamoto, O. Astafiev, Y. Nakamura, D. V. Averin, and J. S. Tsai, Nature (London) **421**, 823 (2003).

[32] O. Astafiev, Y. A. Pashkin, Y. Nakamura, T. Yamamoto, and J. S. Tsai, Phys. Rev. Lett. **93**, 267007 (2004).

[33] Y. Nakamura, Y. A. Pashkin, T. Yamamoto, and J. S. Tsai, Phys. Rev. Lett. **88**, 047901 (2002).

[34] D. Vion, A. Aassime, A. Cottet, P. Joyez, H. Pothier, C. Urbina, D. Esteve, and M. H. Devoret, Science **296**, 286 (2002).

[35] L. Faoro and L. Viola, Phys. Rev. Lett. **92**, 117905 (2004).

[36] G. Falci, A. D'Arrigo, A. Mastellone, and E. Paladino, Phys. Rev. A **70**, 040101(R) (2004).

[37] H. Gutmann, F. Wilhelm, W. Kaminsky, and S. Lloyd, Quantum Inf. Process. **3**, 247 (2004).

[38] H. Gutmann, F. K. Wilhelm, W. M. Kaminsky, and S. Lloyd, Phys. Rev. A **71**, 020302(R) (2005).

[39] Y. X. Liu, L. F. Wei, J. S. Tsai, and F. Nori, Phys. Rev. Lett. **96**, 067003 (2006).

[40] C.-C. Wang, M. Currie, R. Sobolewski, and T. Y. Hsiang, Appl. Phys. Lett. **67**, 79 (1995).

[41] It was sufficient to run the GRAPE algorithm [13] on a MATLAB platform with 10 randomized initial control sequences for each fixed final time T through 10 000 iterations taking some 250 sec CPU time on a 2.7 MHz 512 MB RAM Athlon processor to give trace fidelities $>1-10^{-3}$. The final pulse shape leading to a fidelity $>1-10^{-9}$ for the shortest T was then obtained in an overnight run with no restriction on the number of iterations.

[42] A polynomial (with real coefficients) of the variable $s := \sigma + i\omega$ is termed a Hurwitz polynomial if its zeros are strictly in the left half-plane [i.e., $\text{Re}(s_0) < 0$], while a modified Hurwitz polynomial may also have zeros that are purely imaginary [$\text{Re}(s_0) \leq 0$].